scientific reports

Check for updates

OPEN

Design and fabrication of a dual laser Raman spectrometer with a single one-dimensional CCD detector

Omid Badkoobe Hezave & Seyed Hassan Tavassoli✉

The combination of two spectrometers in dual-laser Raman devices without the need for moving parts represents a significant advancement. This study focuses on design and fabrication of a dual spectrometer with no moving components, allowing data to be gathered using a single detector. This instrument consists of two Czerny–Turner optical arrangements which is symmetrically merged. Dual spectrometer single detector has two light inputs, each of them, concentrating the light separately on a one linear charge-coupled device detector through two independent optical paths. In this innovative spectrometer design, no optical moving parts are used, and therefore, the wavelength displacement error in repeating the spectroscopic experiment is zero. The independent nature of the optical paths enables the optimization of each spectrometer arrangement without affecting the other. The final spectrometer has a spectral resolution of 4.6 and 6.11 cm^{-1} for Full Width at Half Maximum across the wavelength ranges of 532 to 708 nm and 784.65 to 1100 nm, respectively. Switching between the two different acquisition setups can be done seamlessly and quickly, with the ability to record approximately 2000 spectra per second. Standard neon and mercury-argon lamps' atomic radiation spectra, along with Raman scattering data from a cyclohexane standard sample, were successfully recorded using laser wavelengths of 532 nm and 784.65 nm.

The design and construction of spectrometers with unique capabilities and applications in various scientific fields such as biology, physics, and chemistry are important. Recent studies have focused on integrating multiple spectrometers into a single system, resulting in numerous benefits. These advantages include the ability to use portable systems for quick analysis[1], lower manufacturing costs, fast and precise spectrometry[2,3], and eliminating the need for repetitive wavelength calibration[4,5]. The integration of various molecular and elemental spectroscopy techniques is one of the key focuses in the design and construction of spectrometers[6,7]. Recent articles have discussed the combination of laser-induced breakdown spectroscopy (LIBS) and Raman methods in the Mars rover, resulting in a device capable of capturing a broad range of atomic and molecular data in a compact and lightweight design[8,9]. Additionally, NASA's Super Cam instrument showcased in the Mars probe demonstrated the incorporation of four different remote sensing techniques[10]. Another area of research in specialized spectrometer design involves creating devices with optimized selection intervals for specific applications. In some studies, researchers have developed super-high spectral resolution optical spectrometers with zero coma aberration over a broad wavelength range by using multiple sub-gratings[11–13].

In dual laser Raman systems, it is essential to use two spectrometers to efficiently record the Raman spectrum. Each spectrometer is dedicated to recording the distinct Raman spectrum produced by its respective laser source. The most expensive component of Raman spectrometers is the detector. By using a spectrometer that can record Raman spectra from both lasers with only one detector, cost-effective measures can be taken. Additionally, having a single detector enables easy comparisons of results from both spectrometers. Traditional systems typically use moving gratings to disperse light onto the detector. However, the process of shifting the grating is time-consuming and may lead to calibration errors, requiring frequent recalibrations[14–17]. By using a single spectrometer that covers both laser Raman ranges without any movable parts, the testing process can be significantly sped up. This also eliminates the need for frequent recalibrations, reducing the risk of calibration errors. Another solution for accommodating the required range for two Raman configurations without any moving parts is the Echelle setup. Research indicates that using the Echelle arrangement in Raman spectroscopy may lead to a lower signal-to-noise ratio[18]. Although concentrating the signal on one dimension of the detector

Laser and Plasma Research Institute, Shahid Beheshti University, G. C, Evin, Tehran, Iran. ✉email: h-tavassoli@sbu.ac.ir

can somewhat improve the signal-to-noise ratio (SNR), it does not achieve optimal signal intensity. The inherent weakness of the Raman signal highlights the need for a highly sensitive spectrometer, which is why many researchers prefer theCzerny–Turner (C–T) arrangement in this field[19,20].

To increase flexibility in adjusting the positioning and angle of optical elements, a system that combines two (C–T) configurations is used. This setup meets the need for spectral resolution in the specified range without introducing any additional aberrations[21].

In this paper, two different spectrometer setups have been combined to record spectra in two different Raman ranges: 532 nm to 703 nm and 784.65 to 1100 nm. The developed spectrometer has two light entrance slits in two side-by-side arms. Light enters from each of these entrance slits and then passes into the corresponding C–T spectroscopic setup. After separating the wavelengths by a grating, the light is focused by the corresponding mirror onto a linear image sensor (CCD). Due to the importance of signal-to-noise ratio in Raman spectroscopy, there is no limit on cutting and reducing the dimensions of optical elements in the design. With suitable exposure dimensions, a sufficient signal to noise (SNR) ratio will be achieved.

Contrary to the problem and challenge in the design and optical adjustment of arrangements with moving elements, due to the independence of the two integrated spectrometers in Dual Spectrometer Single Detector (DSSD), there is no limitation in the adjustment of the optical arrangements. The optical adjustment of each spectrometer does not cause any disturbance to the adjustment of the other spectrometer. Each spectrometer is designed independently of each other so that the optical aberrations reach their minimum value and the maximum signal-to-noise is observed in the output.

The standard peaks of neon and mercury-argon lamps, as reported in the National Institute of Standards and Technology (NIST), are used for wavelength calibration[22]. The Raman spectra were recorded using both lasers by using the cyclohexane Raman standard sample[23–26]. The spectral resolution Full Width at Half Maximum (FWHM) is 0.17 nm for the 532 nm -setup and 0.44 nm for the 784 nm setup.

Method

The correlation between the degree of coma aberration and the orientations of the optical components is used to optimize the optical setup[27,28]. In Fig. 1, the angles formed by the incident light beam striking the grating and the angles at which it disperses are illustrated.

According to Eq. (1), these angles are related to the diffraction order and the density of the grating lines[29].

$$d\,(sin\theta_{\,i} + sin\theta_{\,d}) = m\lambda \tag{1}$$

In this equation, λ represents the wavelength of the diffracted light. The angles of the incoming light and the diffracted light, denoted as θ_i and θ_d, correspond to their positions relative to the normal of the grating. Additionally, d indicates the width of the grooves, while m refers to the order of diffraction.

The new method presented in accurate wavelength calibration method for compact CCD spectrometer has been used[30]. In this research, noise reduction is done with the binomial method peaks[31]. The Local Maximum Method is used to identify peaks, and a Gaussian function is then fitted to these peaks.

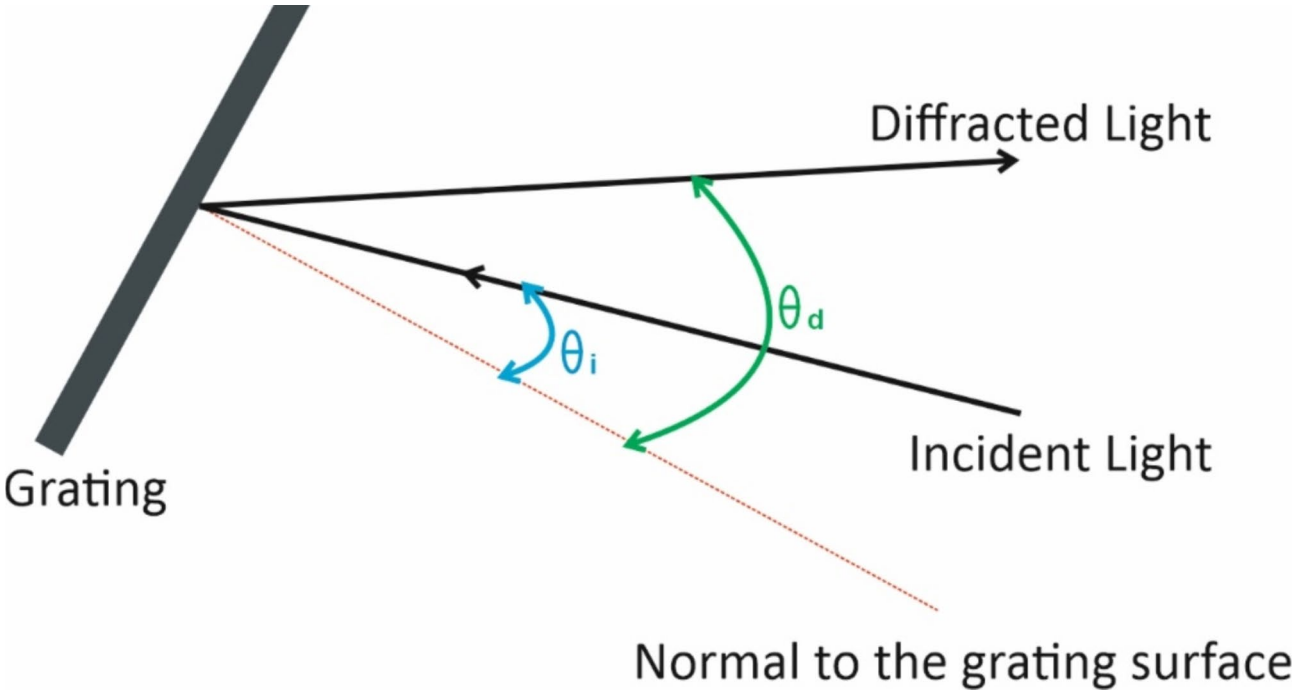

Fig. 1. The optical path along the surface of the grating.

In order to remove unwanted background fluorescence from a Raman spectrum, the second derivative method is utilized to establish a polynomial function that effectively reduces this interference. By implementing this approach, the background is effectively subtracted from the Raman spectrum, enabling more precise identification of Raman peaks.

The initial wavelength range of 784.56 nm on the active area of the detector matches perfectly with the final wavelength range of 532 nm arrangement. Therefore, the data obtained from the 784.65 nm setup is inversely related to that from the 532 nm setup. Consequently, when transitioning between these two setups to collect data, the spectrum is presented in a mirrored fashion.

Experimental configuration

The Schematic illustration of the dual laser Raman setup is shown in Fig. 2. In this setup, the Raman spectra produced by both lasers are collected into optical fibers. The Raman spectrum generated by the 532 nm laser is passed through the optical fiber and fed into the input Slit. Similarly, the Raman spectrum produced by the 784.65 nm laser is directed into the entrance slit port of its corresponding setup using another optical fiber. The lasers are individually activated, with only one laser directed towards the sample through the optical pathway at a time. The two C–T arrays are positioned symmetrically next to each other, with the detector placed directly in the center between them. The second mirror in each spectrometer is connected to a column holder to ensure that the central wavelength light focuses on the detector perpendicularly. By using vertically mounted mirrors on a column to concentrate the dispersed light from the gratings, the entire system was made more compact and efficient.

The optical plane includes points such as the central points of the mirrors, the diffraction grating, the midpoint of the slit, and the horizontal line that intersects the midpoint of the detector and is parallel to its length. The optical plane is tilted by 10 degrees around the axis that passes through the center of the detector pixel array. Both configurations of the spectrometer have a 10-degree angle, with the angles facing in opposite directions. This modification was made without adjusting the angles of the optical components in the spectrometer's optical plane or affecting the second set of mirrors. In Fig. 3, the angle between the horizontal plane and the optical plane is shown. When looking at the detector from the front, the wavefront of the light beam input setup emitting from entrance slit of 532 nm setup is oriented downward, while the light input setup from entrance slit of 784.65 nm setup is oriented upward. When the rotation angle reaches zero degrees, the optical plane aligns perfectly with the horizontal plane, making the spectrometer comparable to traditional spectrometers.

The slit inputs in both Raman setups are 25 microns in size. Spherical mirrors with a diameter of 25 mm and a focal length of 100 mm are utilized. The gratings have a square shape measuring 25 × 25 mm. The Raman grating setups 532 nm and 784.65 nm have line densities of 1200 and 600 lines per millimeter, respectively. The Raman spectrum was recorded using the TCD1304DG sensor, known for its exceptional sensitivity and low dark current. This high-performance detector has 3648 pixels, each measuring 200 × 8 microns, arranged along a single dimension. The sensor can detect wavelengths from 400 nm to 1100 nm, covering the required range for dual laser Raman spectroscopy, specifically 532 nm to 708 nm and 784.65 nm to 1100 nm.

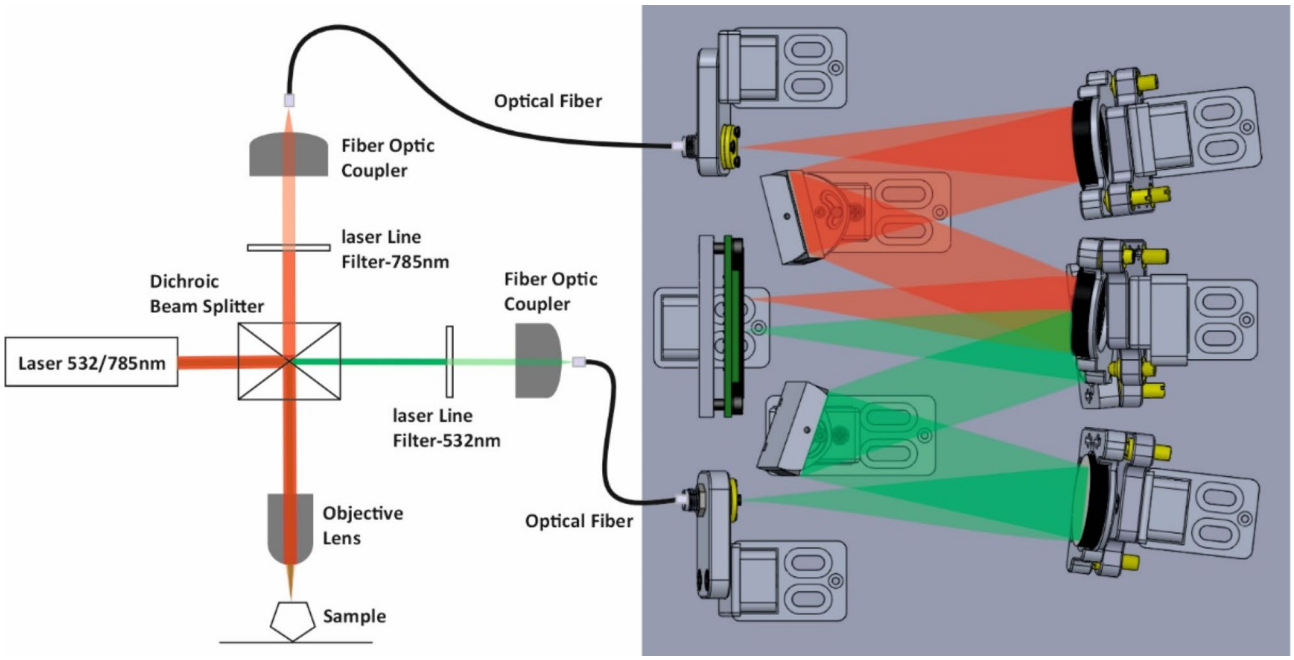

Fig. 2. On the left side of the image is a schematic representation of the Raman setup, and the schematic of the DSSD setup is shown on the right side.

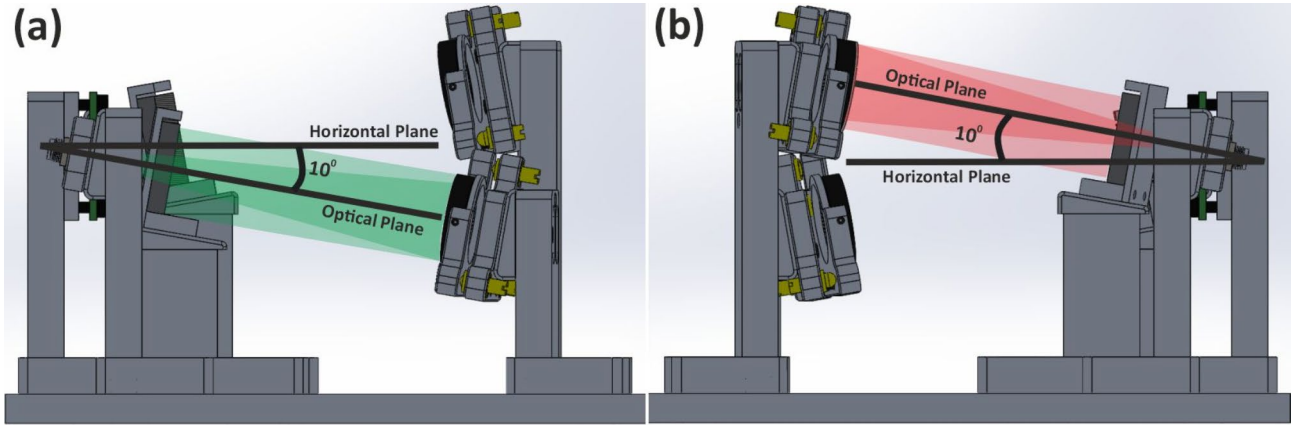

Fig. 3. Associative angle between the horizontal plane and the optical plane in a DSSD configuration: (**a**) for the 532 nm arrangement and (**b**) for the 784.65 nm arrangement.

Results and discussion

An operational prototype of a spectrometer has successfully been constructed, with precise measurements of 180 mm in length, 180 mm in width, and 122 mm in height. The emission spectra of mercury-argon and neon lamps that emit standard radiation were recorded using two different setups. One end of the optical fiber was connected to the light source, while the other end was connected to the selected input slit during the measurement. In Fig. 4, the radiation spectrum of standard lamps and the Raman spectrum of the standard sample of cyclohexane are illustrated. These spectra have been refined using the binomial smoothing method to reduce noise. Additionally, to further reduce noise, each Raman spectrum has been averaged five times, and each radiation spectrum from the standard lamp has been averaged 100 times. A second derivative method has been used to accurately analyze the Raman spectrum, eliminating background spectrum during the fitting process.

The spectrum illustrated in the Fig. 4a from 532 nm setup revealed closely positioned mercury lines at 576.96 nm and 579.066 nm, as well as neon lines at 614.306 nm and 616.359 nm, which were distinctly separated without any overlapping. Additionally, upon closer analysis of the Raman spectrum of the cyclohexane standard sample using the 532 nm laser, distinct peaks were identified at 2923.8 and 2938.3 cm^{-1}. This Raman spectrum is shown in Fig. 4b. Similarly, as shown in Fig. 4c, the spectral lines recorded by the 784.65 nm setup, demonstrated the ability to distinguish closely located lines for neon and argon lamps at wavelengths of 841.843 nm, 840.82 nm, and 842.47 nm. Furthermore, the Raman spectrum of the cyclohexane sample, obtained using a 784.65 nm laser, exhibits peaks at 2923.8 cm^{-1} and 2938.3 cm^{-1}, as illustrated in the spectrum shown in Fig. 4d.

To evaluate the effect of a 10-degree tilt in the optical plane on spectral resolution, we analyzed the experimental data collected from spectrometer and compared it with the theoretical predictions. The peaks in the experimental spectra were identified using the local maximum peaking method. Subsequently, these peaks were analyzed by fitting a Gaussian function to determine their widths. Our data analysis reveals an average resolution (FWHM) spectral width of 0.17 nm for the 532 nm configuration, and the 784.65 nm configuration yielded a width of 0.44 nm. The fitted Gaussian curves for the peaks corresponding to the neon and mercury lamps are illustrated in Fig. 5a and b, respectively. Notably, the peak for the neon lamp, located at a wavelength of 616.39 nm, represents the experimental outcome for the 532 nm setup, and the peak for the mercury lamp at 912.37 nm reflects the experimental result for the 784.65 nm setup.

The determination of spectral resolution in a C–T spectrograph is conducted using (2). Initially, for theoretical calculations, it is assumed that the angle formed by the optical plane is zero. Subsequently, Eq. (2) is used to calculate the average spectral resolution across the entire spectral range[32].

$$FWHM = \left(\frac{dl}{d\lambda}\right)^{-1} MW_S \tag{2}$$

In this equation, M represents the tangential magnification of the entrance slit, which is determined by the focal length F_2 of the second concave mirror, divided by the focal length F_1 of the first concave mirror[33]. This relationship can be expressed mathematically as $M = \frac{F_2}{F_1} = 1$. Here, W_s denotes the width of the entrance slit and the term $\frac{dl}{d\lambda}$ signifies the linear dispersion of the spectrometer. The process outlined in deriving Eq. (1) provides a method for calculating this value.

$$\frac{dl}{d\lambda} = \frac{F_2 m}{d\sqrt{(1 - sin^2\theta_d)}} \tag{3}$$

By substituting Eq. (3) into Eq. (2) and calculating θ_d using Eq. (1), the spectral resolution determines using Eq. (4).

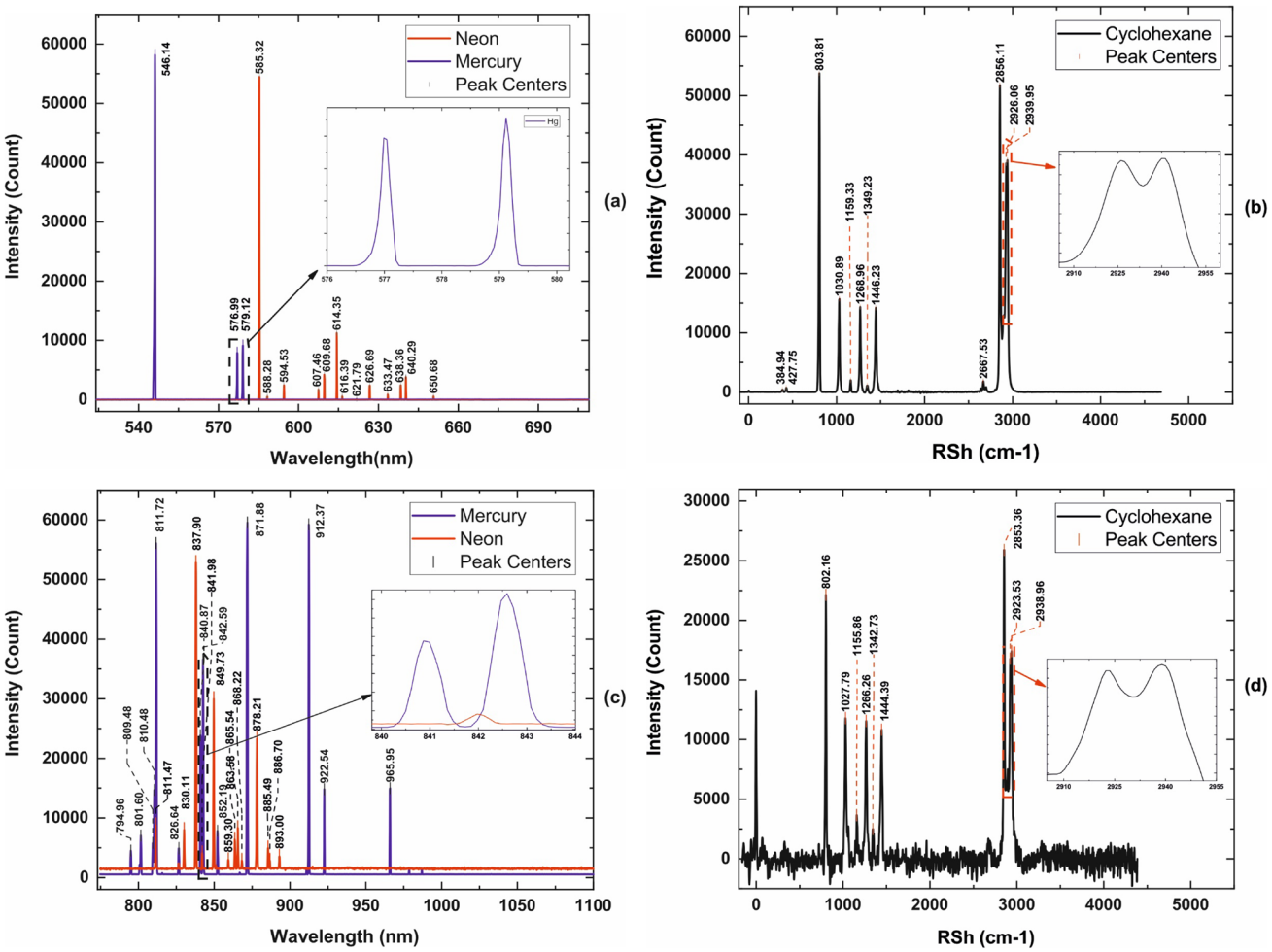

Fig. 4. (**a**) and (**b**) represent the radiation spectrum of standard lamps and the Raman spectrum obtained from a cyclohexane sample using a 532 nm setup. Similarly, the spectra recorded with the 784.65 nm configuration are included in the (**c**) and (**d**).

$$FWHM = \left[\frac{F_2 m}{d\sqrt{1 - sin^2\left(sin^{-1}\left(\frac{m\lambda}{d} - sin\theta_i\right)\right)}}\right]^{-1} W_s \tag{4}$$

According to the spectral resolution results presented in Table 1, creating a 10-degree angle for the optical plane has a negligible effect on the spectral resolution. Optical aberrations play a crucial role in degrading the spectral resolution of a spectrometer, leading to discrepancies between theoretical predictions and experimental measurements. Spherical mirrors inherently exhibit both spherical aberrations and astigmatism, which cannot be entirely eliminated; however, certain techniques can effectively reduce the impact of astigmatism[28,34–38]. Coma aberration, while somewhat manageable using Shaffer's equation, can only be minimized at specific wavelengths, making it impossible to eliminate across the entire spectrum[12,39,40].

According to the Lambert's cosine law, the intensity level increased by a significant 10 degrees when taking into account the cosine coefficient[41]. This is approximately equivalent to 98.5% of the intensity level at a zero-degree angle.

The relation of wavelength in terms of pixel number, which is obtained by fitting a 3rd degree polynomial function on the standard atomic peaks, shows the relationship between each pixel of the detector and the wavelength. This is expressed as an Eq. (5).

$$\lambda_p = C + C_1 P + C_2 P^2 + C_3 P^3 \tag{5}$$

where P represent the pixel number, λ signify the wavelength associated with pixel P, C denote the wavelength for pixel 0. The factors C_1, C_2 and C_3 correspond to the first, second and third coefficients, respectively, and are measured in units of (nm/pixel), (nm/pixel^2) and (nm/pixel^3). The results of the third-degree polynomial regression are presented in Table 2. The R-squared value of 1 for the 532 nm setup and the R-squared value

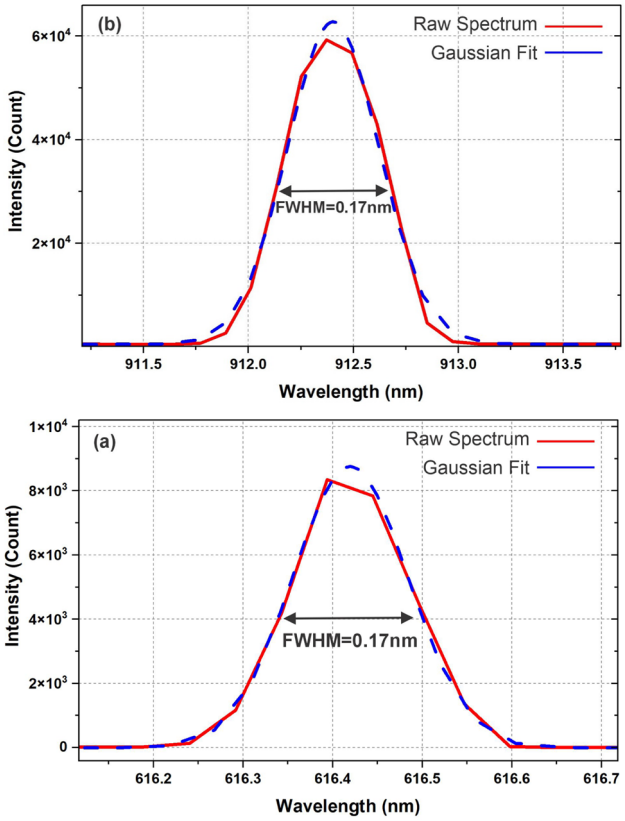

Fig. 5. (**a**) Fitting peak 616.39 nm of neon spectrum, (**b**) Fitting peak 912.3 nm of argon spectrum.

	Theoretical	Theoretical	Experimental	Experimental
configuration	**532 nm**	**784.65 nm**	**532 nm**	**784.65 nm**
FWHM (nm)	0.16	0.36	0.17	0.44
FWHM (cm^{-1})	4.29	4.95	4.60	6.11

Table 1. Theoretical and experimental results of spectral resolution. Significant values are in [bold]

Setup	C	C_1	C_2	C_3	*R* square	Standard error
532	524.2259	0.056006	− 1.3e−6	− 3.8e−11	1	0.020038
784.65	774.809	0.126404	− 2.9e−6	− 2e−11	0.999999	0.061712

Table 2. Results of the third- degree polynomial regression. Significant values are in [bold]

of 0.999999 for the 784.65 nm setup demonstrate the remarkable accuracy of the calibration method used. Additionally, the standard errors associated with the derived coefficients for the polynomial function are 0.020038 for the 532 nm setup and 0.061712 for the 784.65 nm setup, respectively.

To determine the intensity value of the Raman spectrum, we use the signal-to-noise ratio. The signal is represented by the height of the peak at 801 cm^{-1} in the Raman spectrum of the cyclohexane sample. In contrast, the noise is quantified by measuring the standard deviation from the baseline in a region of the Raman spectrum where no peaks are present. The ratio of these two measurements from two distinct Raman spectra illustrates the SNR relationship[42,43]. Based on this analysis, it was found that the SNR ratio for the setup using the 532 nm laser is 7145, while the ratio for the arrangement with the 784.65 nm laser is 40.

This unique setup can be used in both Fluorescence Correlation Spectroscopy (FCS) and Raman Correlation Spectroscopy (RCS) systems which can be considered in future researches[44,45]. Furthermore, using a two-dimensional detector enables the simultaneous record of four Raman spectra.

Conclusion

This paper describes the development of a spectrometer with two entrance slits for light, specifically designed for dual laser Raman spectroscopy device. The instrument uses two lasers with wavelengths of 532 nm and 784.65 nm, covering Raman shift ranges of 0 to 4686 cm^{-1} and 0 to 4386 cm^{-1}, respectively. By incorporating a 10-degree angle in the optical setup, there is negligible impact on both the spectral resolution and intensity of the output spectrum. Switching between two selected modes for recording and displaying spectra is achieved in a fraction of a second. Importantly, the system does not have any optical moving parts, reducing the risk of wavelength errors during spectral measurements. With the dimensions of the optical components maintained, the spectrometer records a sufficient signal-to-noise ratio in the Raman spectrum. The average resolution (FWHM) of line spectra in the 532 nm Raman range is 0.17 nm (equivalent to 4.6 cm^{-1}), and the spectral resolution for the 784.65 nm Raman range is 0.44 nm (equivalent to 6.11 cm^{-1}). The integration time required for spectroscopy in this setup is 500 µs for both configurations.

Data availability

The datasets used and/or analysed during the current study available from the corresponding author on reasonable request.

Received: 18 September 2024; Accepted: 13 November 2024
Published online: 15 November 2024

References

1. Gupta, S. et al. Portable Raman leaf-clip sensor for rapid detection of plant stress. *Sci. Rep.* **10**(1). https://doi.org/10.1038/s41598-020-76485-5 (2020).
2. Mohr, C., Spencer, C. L. & Hippler, M. Inexpensive Raman spectrometer for undergraduate and graduate experiments and research. *J. Chem. Educ. vol.* **87**(3), 326–330. https://doi.org/10.1021/ed800081t (2010).
3. Cho, Y. C. & Il Ahn, S. Fabricating a Raman spectrometer using an optical pickup unit and pulsed power. *Sci. Rep. vol.* **10**(1). https://doi.org/10.1038/s41598-020-68650-7 (2020).
4. Han, T. et al. A new spectrometer using multiple gratings with a two-dimensional charge-coupled diode array detector. *Rev. Sci. Instrum. vol.* **74**(6), 2973–2976. https://doi.org/10.1063/1.1573744 (2003).
5. Liu, M. H. et al. Path-folded infrared spectrometer consisting of 10 sub-gratings and a two-dimensional InGaAs detector. *Opt. Express.* **17**, 14956. https://doi.org/10.1364/OE.17.014956 (2009).
6. Hoehse, M. et al. A combined laser-induced breakdown and Raman spectroscopy Echelle system for elemental and molecular microanalysis. *Spectrochim Acta Part. B Spectrosc.* **64**, 11–12. https://doi.org/10.1016/j.sab.2009.09.004 (2009).
7. Lin, Q., Niu, G., Wang, Q., Yu, Q. & Duan, Y. Combined laser-induced breakdown with Raman spectroscopy: historical technology development and recent applications. *Appl. Spectrosc. Rev.* **48**(6), 487–508. https://doi.org/10.1080/05704928.2012.751028 (2013).
8. Ahlers, B., Hutchinson, I. & Ingley, R. Combined Raman/LIBS spectrometer elegant breadboard: built and tested—and flight model spectrometer unit', SPIE-Intl. *Soc. Opt. Eng.* 110. https://doi.org/10.1117/12.2308293 (2017).
9. Courrèges-Lacoste, G. B., Ahlers, B. & Pérez, F. R. Combined Raman spectrometer/laser-induced breakdown spectrometer for the next ESA mission to Mars. *Spectrochim Acta Mol. Biomol. Spectrosc.* **68**(4), 1023–1028. https://doi.org/10.1016/j.saa.2007.03.026 (2007).
10. Perez, R. et al. The supercam instrument on the NASA Mars 2020 mission: optical design and performance. *SPIE-Intl Soc. Opt. Eng.* 266. https://doi.org/10.1117/12.2296230 (2017).
11. Jiang, A. Q. et al. Ultrahigh-resolution spectrometer based on 19 integrated gratings. *Sci. Rep.* **9**(1). https://doi.org/10.1038/s41598-019-46792-7 (2019).
12. Tu, H. T. et al. A coma-free super-high resolution optical spectrometer using 44 high dispersion sub-gratings. *Sci. Rep.* **11**(1), 1–9. https://doi.org/10.1038/s41598-020-80307-z (2021).
13. Bykov, S. V., Sharma, B. & Asher, S. A. High-throughput, high-resolution echelle deep-UV Raman spectrometer. *Appl. Spectrosc.* **67**(8), 873–883. https://doi.org/10.1366/12-06960 (2013).
14. Berg, R. & Nørbygaard, T. Wavenumber calibration of CCD detector Raman spectrometers controlled by a sinus arm drive. *Appl. Spectrosc. Rev.* **41**(2), 165–183. https://doi.org/10.1080/05704920500510786 (2006).
15. 'Procedures for. wavelength calibration and spectral response correction of CCD array spectrometers 2009&#8217.
16. Scotti, F. & Bell, R. E. High accuracy wavelength calibration for a scanning visible spectrometer. *Rev. Sci. Instrum.* https://doi.org/10.1063/1.3489975 (2010).
17. Liu, D. & Hennelly, B. M. Improved wavelength calibration by modeling the spectrometer. *Appl. Spectrosc. vol.* **76**(11), 1283–1299. https://doi.org/10.1177/00037028221111796 (2022).
18. Pelletier, M. J. 'Raman Spectroscopy Using an Echelle Spectrograph with CCD Detection', Accessed: Mar. 08, 2024. [Online]. Available: (1990). https://doi.org/10.1366/0003702904417580
19. 'Design Simulation of Czerny–Turner Configuration-Based Raman Spectrometer Using Physical Optics Propagation Algorithm Enhanced Reader.pdf'.
20. Futamata, M., Takenouchi, T. & Katakura, K. Highly efficient and aberration-corrected spectrometer for advanced Raman spectroscopy. *Appl. Opt.* **41**, 4655. https://doi.org/10.1364/AO.41.004655 (Aug. 2002).
21. Czerny, M. & Turner, A. F. Über Den Astigmatismus Bei Spiegelspektrometern. *Z. für Physik.* **61**, 11–12. https://doi.org/10.1007/BF01340206/METRICS (1930).
22. Sansonetti, J. E. & Martin, W. C. Handbook of basic atomic spectroscopic data. *J. Phys. Chem. Ref. Data.* **34**(4), 1559–2259. https://doi.org/10.1063/1.1800011 (2005).
23. 'Standard Guide for Raman Shift Standards for Spectrometer Calibration 1', https://doi.org/10.1520/E1840-96R22
24. Hutsebaut, D., Vandenabeele, P. & Moens, L. Evaluation of an accurate calibration and spectral standardization procedure for Raman spectroscopy. *Analyst.* **130**(8), 1204–1214. https://doi.org/10.1039/b503624k (2005).
25. Norlen, G. & Humphreys by 'Wavelengths and Energy Levels of Ar I and Ar II based on New Interferometric Measurements in the Region 3 400-9 800 Å Wavelengths and Energy Levels of Ar I and Ar II based on New Interferometric Measurements in the Region 3400-9 800 a', 1973. [Online]. Available: http://iopscience.iop.org/1402-4896/8/6/007.
26. Burns, K., Adams, K. B. & Longwell, J. 'Interference Measurements in the Spectra of Neon and Natural Mercury'.
27. Shafer, A. B., Megill, L. R. & Droppleman, L. Optimization of the Czerny–Turner Spectrometer*. *J. Opt. Soc. Am.* **54**(7), 879. https://doi.org/10.1364/JOSA.54.000879 (1964).
28. Shafer, A. B. 'Correcting for Astigmatism in the Czerny–Turner Spectrometer and Spectrograph', (1967).
29. Demtröder, W. *Laser Spectroscopy 1: Basic Principles* vol. 9783642538599 (Springer-, 2014). https://doi.org/10.1007/978-3-642-53859-9

30. Sun, Y. C., Huang, C., Xia, G., Jin, S. Q. & Lu, H. B. Accurate wavelength calibration method for compact CCD spectrometer. *J. Opt. Soc. Am. A.* **34**(4), 498. https://doi.org/10.1364/josaa.34.000498 (2017).
31. '1983RevSciInstr_MarchandMarmet_BinomialFilterPitfalls&#8217.
32. Mohammadi, H. & Eslami, E. Investigation of spectral resolution in a czerny turner spectrograph. *Instrum. Exp. Tech. vol.* **53**(4), 549–552. https://doi.org/10.1134/S0020441210040147 (2010).
33. Liu, C. & Berg, R. W. Determining the spectral resolution of a charge-coupled device (CCD) Raman instrument. *Appl. Spectrosc. vol.* **66**(9), 1034–1043. https://doi.org/10.1366/11-06508 (2012).
34. Lee, K. S., Thompson, K. P. & Rolland, J. P. Broadband astigmatism-corrected Czerny–Turner spectrometer. *Opt. Express.* **18**(22), 23378. https://doi.org/10.1364/oe.18.023378 (2010).
35. Xia, G., Wu, S., Wang, G., Hu, M. & Xing, J. Astigmatism-free Czerny–Turner compact spectrometer with cylindrical mirrors. *Appl. Opt.* **56**(32), 9069. https://doi.org/10.1364/ao.56.009069 (2017).
36. An, Y., Sun, Q., Liu, Y., Li, C. & Wang, Z. Q. The design of astigmatism-free crossed Czerny–Turner spectrometer. *Optik* **124**(16), 2539–2543. https://doi.org/10.1016/j.ijleo.2012.07.009 (2013).
37. González-Núñez, H., Montero-Orille, C. & de la Fuente, R. 'Astigmatism in the basic Offner spectrometer', *Optik* **247**, (2021). https://doi.org/10.1016/j.ijleo.2021.167873
38. Xia, C., Zeng, C. & Feng Design of optical system of crossed astigmatism Czerny–Turner spectrometer. *SPIE-Intl Soc. Opt. Eng.* 35. https://doi.org/10.1117/12.2606812 (2021).
39. Chen, T. A., Tang, Y., Zhang, L. J., Chang, Y. E. & Zheng, C. Correction of astigmatism and coma using analytic theory of aberrations in imaging spectrometer based on concentric off-axis dual reflector system. *Appl. Opt.* **53**(4), 565. https://doi.org/10.1364/ao.53.000565 (2014).
40. Allemand, C. D. 'Coma Correction in Czerny–Turner Spectrographs', (1968).
41. 'Optical Design for Biomedical Imaging'. [Online]. Available: http://spiedl.org/terms
42. Bentz, C. M., Baudzus, L. & Krummrich, P. M. Signal to noise ratio (SNR) enhancement comparison of impulse-coding-and novel linear-frequency-chirp-based optical time domain reflectometry (OTDR) for passive optical network (PON) monitoring based on unique combinations of wavelength selective mirrors. *Photonics* 1(1), 33–46. https://doi.org/10.3390/photonics1010033 (2014).
43. McCreery, R. L. 'Raman Spectroscopy for Chemical Analysis', in *Raman Spectroscopy for Chemical Analysis*, New York I Chichester I Weinheim I Brisbane I Singapore I Toronto: Wiley, doi: (2000). https://doi.org/10.1002/0471721646.fmatter
44. Bacia, K., Kim, S. A. & Schwille, P. Fluorescence cross-correlation spectroscopy in living cells. *Nat. Methods 2006 3:2* **3**(2), 83–89. https://doi.org/10.1038/nmeth822 (2006).
45. Schrof, W., Klingler, J., Rozouvan, S. & Horn, D. Raman correlation spectroscopy: A method for studying chemical composition and dynamics of disperse systems. *Phys. Rev. E.* **57**(3), R2523. https://doi.org/10.1103/PhysRevE.57.R2523 (1998).

Author contributions

S. has played a crucial role in establishing the optical setup and optimizing the spectrum. His guidance has been instrumental in selecting optical instruments and designing their supports. Additionally, he provided valuable feedback and suggestions for improving the article's writing.O. has created the designs for the optical holders and conducted all the necessary calculations for the optical layout. Additionally, he has performed optical adjustments, carried out experiments, processed the output data, and completed the final calculations. He also authored the article and prepared the accompanying images and tables.

Declarations

Competing interests

The authors declare no competing interests.

Additional information

Correspondence and requests for materials should be addressed to S.H.T.

Reprints and permissions information is available at www.nature.com/reprints.

Publisher's note Springer Nature remains neutral with regard to jurisdictional claims in published maps and institutional affiliations.